Layered-Double-Hydroxide Nanosheets as Efficient Visible-Light-Driven Photocatalysts for Dinitrogen Fixation

Yufei Zhao, Yunxuan Zhao, Geoffrey I. N. Waterhouse, Lirong Zheng, Xingzong Cao, Fei Teng, Li-Zhu Wu, Chen-Ho Tung, Dermot O'Hare, and Tierui Zhang*

Semiconductor photocatalysis attracts widespread interest in water splitting, CO_2 reduction, and N_2 fixation. N_2 reduction to NH_3 is essential to the chemical industry and to the Earth's nitrogen cycle. Industrially, NH_3 is synthesized by the Haber–Bosch process under extreme conditions (400–500 °C, 200–250 bar), stimulating research into the development of sustainable technologies for NH_3 production. Herein, this study demonstrates that ultrathin layered-double-hydroxide (LDH) photocatalysts, in particular CuCr-LDH nanosheets, possess remarkable photocatalytic activity for the photoreduction of N_2 to NH_3 in water at 25 °C under visible-light irradiation. The excellent activity can be attributed to the severely distorted structure and compressive strain in the LDH nanosheets, which significantly enhances N_2 chemisorption and thereby promotes NH_3 formation.

Semiconductor photocatalysis attracts widespread interest due to its potential to capture solar energy and drive thermodynamically unfavorable chemical reactions, such as water

Dr. Y. F. Zhao, Y. X. Zhao, Prof. L.-Z. Wu, Prof. C.-H. Tung, Prof. T. Zhang
Key Laboratory of Photochemical Conversion
and Optoelectronic Materials
Technical Institute of Physics and Chemistry
Chinese Academy of Sciences
Beijing 100190, P. R. China
E-mail: tierui@mail.ipc.ac.cn

Y. X. Zhao
University of Chinese Academy of Sciences
Beijing 100049, P. R. China

Y. X. Zhao, Prof. F. Teng
School of Environmental Science and Engineering
Nanjing University of Information Science and Technology
Nanjing 100084, P. R. China

Prof. G. I. N. Waterhouse
School of Chemical Sciences
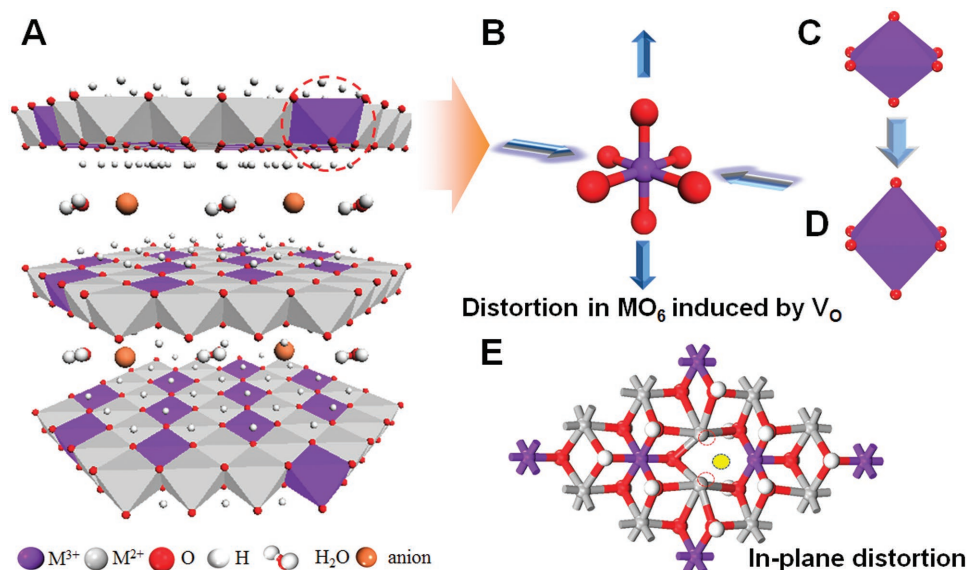The University of Auckland
Auckland 1142, New Zealand

Prof. L. Zheng, Prof. X. Cao
Institute of High Energy Physics
Chinese Academy of Sciences
Beijing 100049, P. R. China

Prof. D. O'Hare
Chemistry Research Laboratory
Department of Chemistry
University of Oxford
Mansfield Road, Oxford OX1 3TA, UK

The ORCID identification number(s) for the author(s) of this article can be found under https://doi.org/10.1002/adma.201703828.

splitting, CO_2 reduction, and N_2 fixation. To drive these reactions, a photocatalyst must efficiently absorb solar energy to generate an abundance of charge carriers (electron–hole pairs), quickly separate these charge carriers to minimize recombination, adsorb reactants strongly to enable reaction with migrating carriers, and have valence and conduction band energies appropriate for the oxidation and reduction reactions, respectively.[1] Inspired by the excellent photoactivities and turnover frequencies of many enzymes and biomolecules with coordinately unsaturated metal sites, such as [Fe–Fe] nitrogenase,[2] biomimetic Mo/Fe sulfides,[3] and CdS:MoFe proteins,[4] researchers have sought to introduce defect sites into traditional semiconductors[5] like TiO_2,[6] $BiOBr/Cl$,[7] WO_3,[8] and Au/silicon[9] as a means of activating H—O, C=O, and N≡N bonds under appropriate photoexcitation.[10] However, most traditional photocatalysts have inherent limitations in terms of the concentration of defects that can be introduced as active adsorption sites, while also generally exhibiting weak visible-light absorption around 420–500 nm,[1] severely handicapping their solar spectrum utilization efficiency.

Recently, 2D ultrathin nanosheet photocatalysts have emerged as a very promising new category of semiconductor photocatalysts,[11] intrinsically containing an abundance of surface defects such as oxygen vacancies (V_O), thereby exposing coordinately unsaturated metal sites that increase in concentration as the thickness of photocatalysts approaches atomic scales (i.e., ≈1 nm).[12] Defect engineering via the 2D approach creates new active sites for reactant adsorption and can also increase visible-light absorption through narrowing the bandgap, synergistically enhancing photocatalytic activity. For example, oxobridged heterobinuclear units like Ti/Zr—O—Cr/Co/Cu/Sn on silica were shown by Frei and co-workers and Hashimoto and co-workers possess metal-to-metal charge-transfer (MMCT) absorption bands that act as deep visible-light absorbing chromophores for photocatalysis.[13] Layered double hydroxides (LDHs) represent a new class of MMCT-based system[14] and have very promising for photocatalytic applications due to their easily controllable metal cation composition and thicknesses that allows both defect engineering and bandgap tuning.[15] LDHs are composed of sheets of edge sharing MO_6 octahedra and are commonly described by the general formula $[M_{1-x}^{2+}M_x^{3+}(OH)_2]^{q+}(A^{n-})_{q/n} \cdot \gamma H_2O$ (where $M^{2+} = Mg^{2+}$, Co^{2+},

Scheme 1. A) Schematic polyhedral representation of the ultrathin LDH structure with defective MO_6 octahedra at the nanosheet edge or surface. B) Biaxial strain for MO_6 octahedra in LDH nanosheets. C,D) Undistorted MO_6 octahedron (C) and the corresponding strained MO_6 octahedron (D). E) 2D structural model for an LDH monolayer from DFT calculations viewed from above (V_O marked by the yellow dot).

Ni^{2+}, Cu^{2+} or Zn^{2+}; M^{3+} = Al^{3+} or Cr^{3+}; and A^{n-} are charge balancing anions located between sheets). By synthesizing LDH nanosheets only a few nanometers thick, V_O can be easily generated on the surface/edge of the nanosheets. In a recent study, we successfully demonstrated that V_O-doped ZnAl-LDH nanosheets can simultaneously activate C=O and H−O bonds in CO_2 and H_2O, respectively, under UV excitation, resulting in the formation of CO and O_2.[16] By tuning the composition (i.e., the divalent and trivalent cations) and morphology (thickness and lateral dimensions) of LDH nanosheets, it should also be possible to generate coordinately unsaturated sites for photocatalytic activation of other challenging molecules like N_2 under visible light. To our knowledge, no prior work has been reported examining the photocatalytic performance of ultrathin LDH-based photocatalysts for N_2 fixation, motivating a detailed investigation.

The catalytic reduction of dinitrogen (N_2) with hydrogen (H_2) to ammonia (NH_3) in the Haber–Bosch process is a fundamental pillar of today's chemical industry, and was first demonstrated in 1913.[4a,17] The rate-limiting step in the Haber–Bosch process is the dissociation of N_2 to nitrogen atoms, requiring drastic reaction conditions (200–250 bar, 400–500 °C) over Fe-based catalysts to achieve practical surface coverages of chemisorbed nitrogen atoms. H_2 used in the Haber–Bosch process is typically derived by steam methane reforming coupled with the water-gas shift reaction, with the former utilizing a fossil fuel feedstock (CH_4). In view of future fossil fuel shortages and global warming resulting from anthropogenic CO_2 emissions (including those arising from the chemical industry), alternative pathways toward NH_3 are now being actively pursued. Among these, the transformation of N_2 to NH_3 using semiconducting photocatalysts in the presence of sunlight at ambient temperature[18] represents a very promising future synthetic route.[3b,6,7,9,17b,19] However, identification and synthesis of suitable photocatalysts remain a challenge, with the adsorption and

activation of N_2 representing a significant obstacle for photocatalytic ammonia synthesis.

Herein, we demonstrate that $M^{II}M^{III}$-LDH (M^{II} = Mg, Zn, Ni, Cu; M^{III} = Al, Cr) nanosheet photocatalysts strategically engineered with V_O defects and synthesized through simple co-precipitation methods promote the chemisorption and activation of N_2 at ambient temperature and pressure. A CuCr-LDH nanosheet photocatalyst displayed an extraordinarily high activity for the photoreduction of N_2 to NH_3 under visible-light irradiation (even at wavelengths > 500 nm) in the presence of water. The key to this remarkable photocatalytic performance was distortions in the MO_6 octahedra caused by the introduction of V_O within the ultrathin LDH nanosheets (**Scheme 1**), as revealed by X-ray absorption fine structure (XAFS) and position annihilation spectroscopy (PAS) measurements. Density functional theory (DFT) calculations indicate that V_O introduces gap states that promote N_2 adsorption and facilitate photo-induced charge transfer from LDH to N_2, while also serving as active sites for the chemical reaction of N_2 and H_2O to NH_3 and O_2, respectively. This work thus identifies a novel low-energy-input pathway for NH_3 synthesis using 2D photocatalytic LDH materials.

Initially, this study aimed to evaluate the potential of conventional M^{II}Al-LDHs (M^{II} = Mg, Zn, Ni) as photocatalysts. However, during the initial stages of the project, it was reported that group 6 complexes containing Mo, W, and Cr possessed activity for N_2 reduction.[20] Neither Mo^{3+} nor W^{3+} cations can be incorporated into the LDH hydroxide layer, but Cr^{3+} can be accommodated. Since Cr^{3+} shows a strong absorption in the visible-light range, highly beneficial in terms of solar-driven photocatalyst development, Cr^{3+} was selected as an additional trivalent cation for the synthesis of LDH nanosheets. Cu^{2+} was also chosen as a divalent cation in LDH due to the existence of a strong Jahn–Teller effect and thus its potential for introducing defects. $M^{II}M^{III}$-LDH (M^{II} = Mg, Zn, Ni, Cu; M^{III} = Al, Cr)

**ADVANCED
SCIENCE NEWS**
www.advancedsciencenews.com
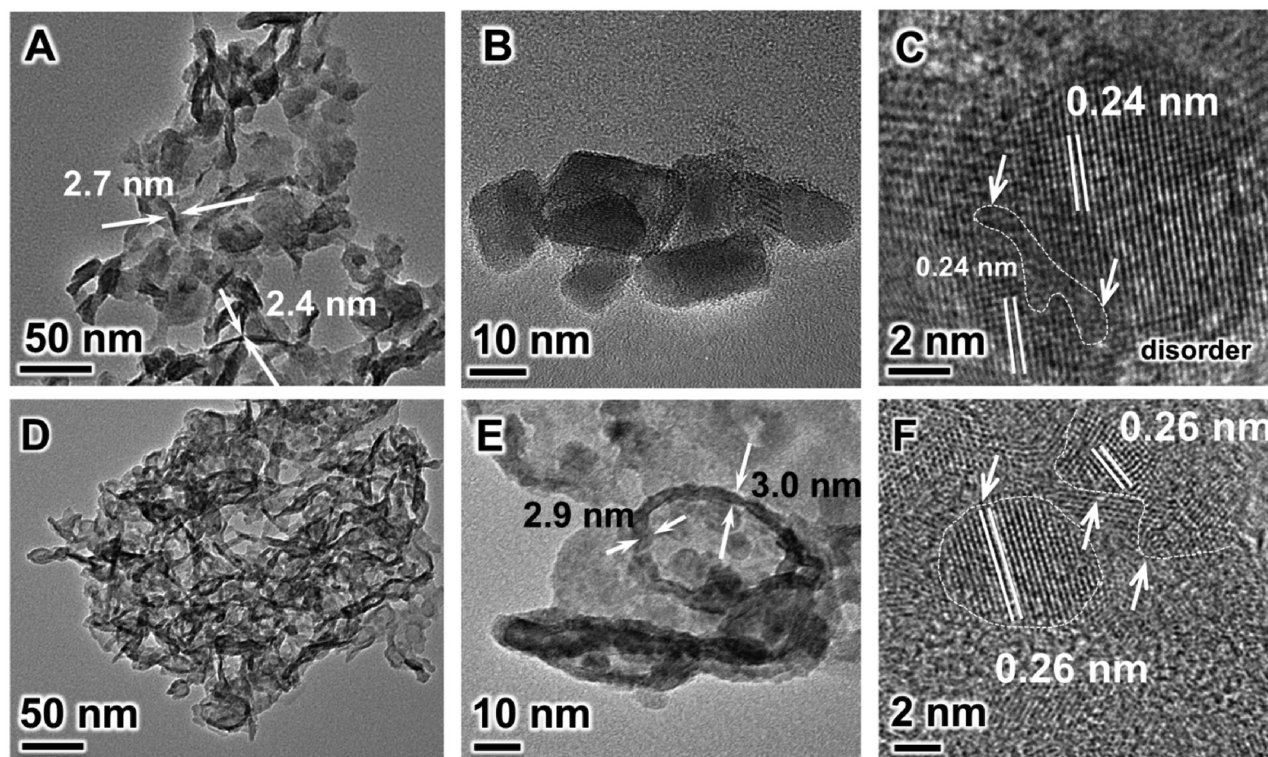
**ADVANCED
MATERIALS**
www.advmat.de

Figure 1. A–C) TEM (A) and HRTEM (B,C) images of CuCr-NS. D–F) TEM (D) and HRTEM (E,F) images of ZnAl-NS.

ultrathin nanosheets (denoted herein as $M^{II}M^{III}$-NS) were all successfully prepared using NaOH as a co-precipitation agent in combination with rapid mixing and a fast nucleation process.[21] Due to the simplicity of the co-precipitation method used here for the $M^{II}M^{III}$-NS syntheses, it is readily amenable to scale up and thus of practical relevance to industry. As shown in Figure S1 (Supporting Information), a harmonic series of Bragg reflections were observed by powder XRD for each $M^{II}M^{III}$-NS which can be indexed to (001) planes of the rhombohedral LDH layer structure.[21] The shift in the position of the (003) Bragg reflection for the various $M^{II}M^{III}$-NS samples can be attributed to nature of the anions (nitrate or carbonate) intercalated in the LDH nanosheets. Transmission electron microscopy (TEM) images of the as-synthesized $M^{II}M^{III}$-NS samples indicate that all the LDH nanosheets have a platelet morphology with a lateral dimension of 20–50 nm (**Figure 1** and Figure S2, Supporting Information), providing direct experimental evidence for the successful synthesis of ultrathin LDH nanosheets. Figure 1A,B shows that the CuCr-NS sample possessed a nanosheet structure with a mean lateral size of ≈20 nm and a thickness of ≈2.5 nm. A homogeneous distribution of both Cu and Cr in the nanosheets was evident from high-angle annular dark field images (Figure S3, Supporting Information). The high-resolution TEM (HRTEM) image of a CuCr-NS nanosheet showed a lattice fringe spacing of 0.24 nm (Figure 1C), referenced to the (009) planes of the LDH structure. Slight lattice disorder and dislocations can be seen in the nanosheet, confirming the existence of defects. The same phenomena were also found in the ZnAl-NS system. It should be noted that the HRTEM images of ZnAl-NS (Figure 1D,E) show

a wrinkled/curved sheet structure, implying a severely disordered arrangement of the atoms in the ultrathin nanosheets. The boundaries of the ZnAl-NS crystals provide further evidence of structural distortions as a consequence of defect sites in the ZnAl-LDH nanosheets (Figure 1F). These structural distortions are universal in ultrathin nanosheet systems due to abundant surface defects, which allow minimization of the total surface energy. Structural distortions allow a more thermodynamically stable structure to be adopted.[11b,22] Compared to conventionally synthesized bulk CuCr-LDH or bulk ZnAl-LDH samples (denoted as CuCr-Bulk or ZnAl-Bulk, respectively) (Figure S2E,F, Supporting Information), the LDH nanosheets with a smaller particle size and shorter crystalline domain length were expected to possess a significantly higher concentration of surface defects (especially V_O), which, in turn, should favorably enhance their catalytic and photocatalytic properties, as is systematically explored in the following sections.

In order to probe the local coordination of metal cations in both the CuCr-LDH and ZnAl-LDH nanosheets and bulk compounds, XAFS spectra were collected, with the results presented in **Figure 2**. Of particular interest was how the MO_6 coordination sphere in the LDH materials changed as the thickness of the LDH crystals approached atomic length scales. X-ray absorption near-edge fine structure (XANES) and extended X-ray absorption fine structure (EXAFS) k-space spectra from Cr cations in CuCr-NS (Figure 2A,B) were similar to those for Cr cations in CuCr-bulk, suggesting a similar octahedral Cr—O coordination. However, it should be noted that pre-edge features provide sensitive information about the coordination symmetry of Cr in octahedral environments, with an
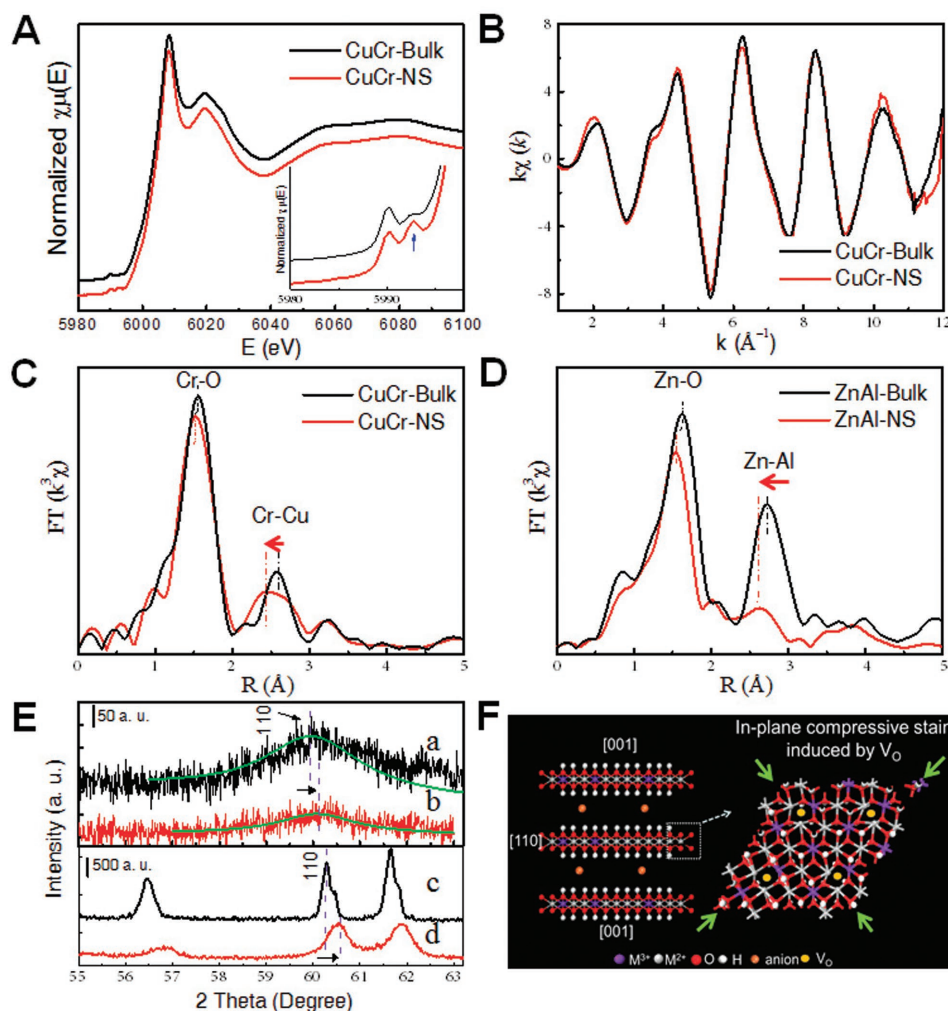
Figure 2. A) Cr K-edge XANES spectra. B,C) Cr K-edge EXAFS oscillation function $k^2\chi$ (k) (B), and magnitude of k^2-weighted FT of Cr K-edge EXAFS spectra (C) for CuCr-Bulk and CuCr-NS. D) Zn K-edge EXAFS spectra for ZnAl-NS and ZnAl-Bulk. E) XRD patterns of CuCr-Bulk (a), CuCr-NS (b), ZnAl-Bulk (c), and ZnAl-NS (d). F) Schematic of the in-plane biaxial compressive strain in the as-synthesized LDH nanosheets.

obvious extra peak around 5993 eV seen for Cr ions in CuCr-NS indicating coordination site disorder (Figure 2A, inset).[23] Furthermore, a significant reduction of the K-edge oscillations was clearly observed between 2–12 Å for the CuCr-NS, again providing evidence of subtle variations in the coordination around the Cr atoms between the nanosheet and bulk counterpart. R space plots yielded detailed information about the Cr—O shell and Cr—O—metal shell in CuCr-NS and CuCr-Bulk. As shown in Figure 2C, the average distance of first Cr—O shell in CuCr-NS is 1.989 Å which is shorter than that observed in CuCr-Bulk (1.990 Å). Further, the reduced coordination number (5.5) for Cr in CuCr-NS compared to CuCr-Bulk (6.0) indicates a severe structural distortion about Cr cations in CuCr-NS, consistent with the formation of abundant V_O. A similar finding was reported recently in NiTi-LDH nanosheet systems.[23] More importantly, due to the first shell effects, the second Cr–Cu distance was reduced from 3.060 Å in CuCr-Bulk to 3.056 Å in CuCr-NS (Table S1, Supporting Information). The same tendency was also seen in the ZnAl-NS system, where the average Zn–Al distance was reduced to 3.068 Å compared to 3.089 Å in

ZnAl-Bulk (Figure 2D and Figure S4, Supporting Information). These results provide solid experimental evidence for a structural compression in the ab-plane in the ultrathin nanosheets. X-ray powder diffraction (XRD) data for the LDH nanosheets and their bulk counterparts lend support to this argument, since the (110) Bragg reflection for both CuCr-NS and ZnAl-NS are observed at higher 2θ angles compared with the corresponding reflection for CuCr-Bulk and ZnAl-Bulk (Figure 2E and Figure S5, Supporting Information), respectively. These data suggest an in-plane biaxial compressive strain in the basal (110) plane for the LDH nanosheet samples. Note that the unit cell lattice constant (a) corresponds to the distance between two metal cations, (i.e., the Cr–Cu or Zn–Al distance parallel to the plane), and thus is closely related to the stoichiometry ratio of M^{II}/M^{III} in the LDH compound. Figure S6 (Supporting Information) compares samples with the same M^{II}/M^{III} ratio in LDH nanosheets and bulk counterparts. From the XRD patterns, we can determine the lattice parameter $a = 2d(110)$, while the lattice parameter $c = 3d(003)$ and is equal to the thickness of one metal hydroxide layer plus one interlayer spacing. From the

Table 1. Unit cell parameters for selected LDH nanosheets and their bulk counterparts.

Sample	d_{110} [Å]	a [Å]	c [Å]	Strain degree around [110] direction
CuCr-NS	1.535	3.070	26.517	−0.20 %
CuCr-Bulk	1.538	3.076	26.423	
ZnAl-NS	1.526	3.052	22.339	−0.46 %
ZnAl-Bulk	1.533	3.066	22.602	

metal to metal distance (a) in the LDHs (**Table 1**), the degree of compression or negative strain around the ab-plane of CuCr-NS was determined to be about 0.20% with respect to CuCr-Bulk, while for ZnAl-NS a negative strain of 0.46% was found compared with the bulk counterpart. The difference between CuCr-NS and ZnAl-NS in c is related to their different interlayer anions (nitrate and carbonate, respectively). The in-plane compressive strain within the LDH nanosheets is further evidence for surface V_O, with the severely structural distortions revealed by XRD helping to lower the surface energy in the ab-plane of the ultrathin nanosheets. The different strain degree seen for CuCr-NS and ZnAl-NS is mainly due to the degree of crystallinity achieved during the synthesis and the relatively different concentration of defect sites compared with their bulk counterparts. Xiang and co-workers also reported compressive strain in MoS_2 nanosheets when compared with bulk MoS_2.[24] The data presented here strongly suggest that LDH nanosheets contain in-plane compressive strain due to an abundance of V_O, as depicted schematically in Figure 2F.

PAS was used to quantify the defect concentration in the Cr-containing LDH samples. As shown in **Table 2**, a positron lifetime τ_1 of around 200 ps can be assigned to bulk defects, whereas the longer lived positrons τ_2 ($\approx$350 ps) can be attributed to surface defects. The largest component (τ_3) is assigned to micropores. By ratioing intensities of the peaks associated with τ_2 and τ_1, the relative surface-to-bulk defect ratio (I_2/I_1) can be obtained. The analysis yielded the following ratios: CuCr-NS (2.52) > ZnCr-NS (2.39). For the CuCr-LDH system, Jahn–Teller distortions will exist due to the presence of Cu(II) ions.[25] Jahn–Teller distortions presumably explain why CuCr-NS possesses a higher concentration of surface defects compared with ZnCr-NS. Generally, LDH nanosheets expose an abundance of surface defects compared with their bulk LDH counterparts, as reported in our previous work.[16] It is well known that surface defects enhance reactant adsorption and promote catalytic activity. From the EXAFS and PAS analyses, it is evident that the LDH nanosheets contain an abundance of surface oxygen defects and compressive bonding due to their thickness being reduced to atomic dimensions. The influence of these surface defects and distortions on N_2 adsorption and transformation to NH_3 are explored below.

Table 2. Positron lifetime parameters for Cr-containing LDH nanosheets.

Sample	τ_1 [ps]	I_1	τ_2 [ps]	I_2	τ_3 [ns]	I_3	I_2/I_1
CuCr-NS	196.8	27.9	347.4	70.2	2.104	1.86	2.52
ZnCr-NS	199.0	28.8	340.9	69.0	2.087	2.18	2.39

Diffuse reflectance UV–vis spectra were collected from the LDH samples to gauge their light absorption ability for subsequent photocatalytic experiments (Figure S7, Supporting Information). All of the Cr-containing LDHs show two visible-light absorption bands centered around 410 and 570 nm, attributed to the d–d transitions $^4A_{2g}(F)\rightarrow{}^4T_{1g}(F)$ (410 nm) and $^4A_{2g}(F)\rightarrow{}^4T_{2g}(F)$ (570 nm) of Cr^{3+} in an octahedral environment in the LDH MO_6 layers.[26] CuCr-NS gives a stronger absorption signal compared with NiCr-NS and ZnCr-NS, due to the additional Cu d–d band transition at 800 nm.[27] The absorption band in the 200–300 nm region originates from electron transitions from O 2p orbital to 3d orbitals of the metal ions.[28] NiAl-NS also exhibits absorption at visible wavelengths due to the presence of Ni^{2+} ions ($3d^8$), whereas ZnAl-LDH and MgAl-LDH contain only the d^0 and d^{10} ions and thus only absorb strongly in the UV region. The colors of the various LDH nanosheet samples (Figure S7B, Supporting Information) are consistent with expectations based on their UV–vis absorption spectra. This controllable optical absorption of LDH materials is due to the oxo-bridged bimetallic linkage of M^{II} and M^{III} (M^{II} = Mg, Zn, Ni, Cu; M^{III} = Al, Cr).[14b,26b]

All the LDH materials were subsequently evaluated for their ability to convert N_2 to NH_3 under UV–vis irradiation. Samples were dispersed in N_2-saturated H_2O, with the water acting as both a proton source (instead of H_2) and solvent for the NH_3 product (**Figure 3**A). Quantitative determination of NH_3 formation was performed via complexation with Nessler's reagent. As shown in Figure 3B and Figure S8A (Supporting Information), almost all the LDH nanosheets were active for NH_3 formation under UV–vis irradiation. The activity followed the order CuCr-NS (184.8 μmol L^{-1}) > NiCr-NS (56.3 μmol L^{-1}) > ZnCr-NS (31.2 μmol L^{-1}) > ZnAl-NS (38.2 μmol L^{-1}) > NiAl-NS (22.3 μmol L^{-1}). MgAl-NS was found to be inactive, presumably due to its wide bandgap ($\approx$5.0 eV).[29] Not surprisingly, based on their colors, most of the LDH nanosheets also exhibit N_2 photofixation activity (Figure 3C) under visible light, with CuCr-NS again demonstrating the best performance (NH_3 evolution rate 142.9 μmol L^{-1}), followed by NiCr-NS (42.1 μmol L^{-1}), ZnCrNS (16.5 μmol L^{-1}), and NiAl-NS (20.0 μmol L^{-1}). As expected, the ZnAl-NS and MgAl-NS samples did not produce any NH_3 due to their wide electronic bandgaps (UV-responsive only). By decreasing the pH of the reaction medium, the NH_3 evolution rate over CuCr-LDH under visible light improved from 35.7 μmol L^{-1} at pH 8.0 to 142.9 μmol L^{-1} at pH 6.9, 175.3 μmol L^{-1} at pH 5.8, and finally 220.9 μmol L^{-1} at pH 5.0 (Figure S8E, Supporting Information). Most LDHs have an isoelectric point of $\approx$9.5. Thus, decreasing pH and increasing availability of protons on the photocatalyst surface enhance NH_3 evolution. CuCr-NS also displayed excellent photocatalytic stability, with no obvious decrease in activity evidenced after five successive photocatalytic cycles (Figure 3D). X-ray photoelectron spectroscopy (XPS) confirmed that the valency of Cu and Cr in CuCr-NS did not change following the reaction (Figure S9, Supporting Information). It should be noted that visible-light-responsive photocatalysts for N_2 fixation are not common, with the remarkable performance demonstrated here by the CuCr-NS, NiCr-NS, ZnCr-NS, and NiAl-NS photocatalysts originating from their 2D defective structure. A control experiment conducted by substituting N_2 with argon (Ar) and using CuCr-NS showed
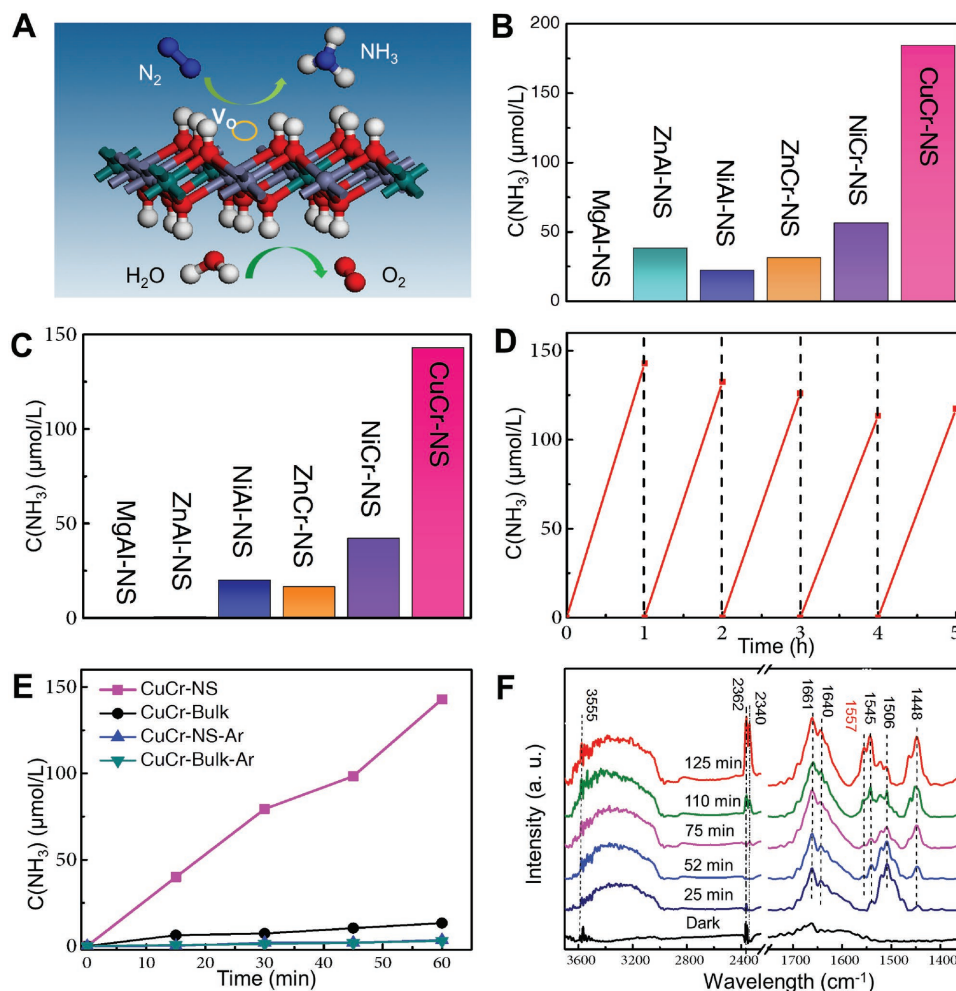
**ADVANCED
SCIENCE NEWS**

www.advancedsciencenews.com

**ADVANCED
MATERIALS**

www.advmat.de

Figure 3. A) Schematic illustrating the photocatalytic N_2 fixation process. B,C) Yield of NH_3 over a 1 h test period for different LDH photocatalysts under UV–vis illumination (B), and visible-light illumination ($\lambda > 400$ nm, PLS-SXE300D) (C) with water as the proton source. D) Catalyst cycling tests for CuCr-NS under N_2 in the presence of water under visible-light illumination. E) Time course of NH_3 evolution in the photofixation of N_2 or argon (Ar) in the presence of water under visible-light illumination over CuCr-NS and CuCr-Bulk. F) In situ IR spectra recorded from CuCr-NS under N_2 and water vapor during 125 min UV–vis illumination.

negligible NH_3 production (Figure 3E), confirming the photofixation of N_2 was indeed responsible for the NH_3 evolution.

In order to track the activation of N_2, in situ diffuse reflectance infrared Fourier transform spectroscopy was applied to identify reaction intermediates on the CuCr-NS surface (Figure 3F). In the presence of N_2 and water vapor under UV–vis irradiation, signals for a number of adsorbed species observed. The peaks at 3600–3000 and ≈1640 cm^{-1} can readily be assigned to adsorbed H_2O (asymmetric stretching and bending modes, respectively). The 2340 and 2362 cm^{-1} absorption bands are similar in frequency to the values (2330 and 2350 cm^{-1}) reported by Domen and co-workers for N_2 adsorption on layered FeTiO-based photocatalysts, suggesting that these features are likely due to a chemisorbed N_2 species.[30] The bands at 1661, 1557, and 1448 cm^{-1} are characteristics for antisymmetric and symmetric deformations of a surface NH_4^+ species (the associated N—H stretching vibrations in the 3200–3600 cm^{-1} region will be obscured by the presence of adsorbed water).[31] O_2 evolution accompanied the photofixation of N_2 over CuCr-NS,

with ≈100 % selectivity to NH_3 being achieved without the formation of N_2H_4 or H_2 (Figure S8B–D, Supporting Information). When LDH absorbs visible light, an electronic excitation occurs referred to as an MMCT transition. The MMCT phenomenon was explored in detail by Parida and co-workers for LDH systems, who reported that upon visible-light irradiation, $Zn^{II}/Ni^{II}/Cu^{II}$–O–Y^{III}/Cr^{III} units transform to $Zn^{I}/Ni^{I}/Cu^{I}$–O–Y^{IV}/Cr^{IV}.[14a] A similar MMCT process was seen for Ti^{IV}–O–Cr^{III}/Mn^{II} assembled on silica, which transformed to Ti^{III}–O–Cr^{IV}/Mn^{III} under visible light.[13c,32] In such cases, surface-adsorbed H_2O can be oxidized to produce protons for the reduction of N_2 to NH_3. During the N_2 photofixation process, V_O on the surface of CuCr-NS (and other active LDH-NS systems) plays a key role in the photocatalytic N_2 fixation process by acting as binding sites for N_2 adsorption, which is discussed in the following section.

In the photocatalytic tests described above, the LDH nanosheets demonstrated superior photocatalytic N_2 reduction activity compared with their bulk counterparts. The origin of this superior activity is clearly related to the LDH nanosheet
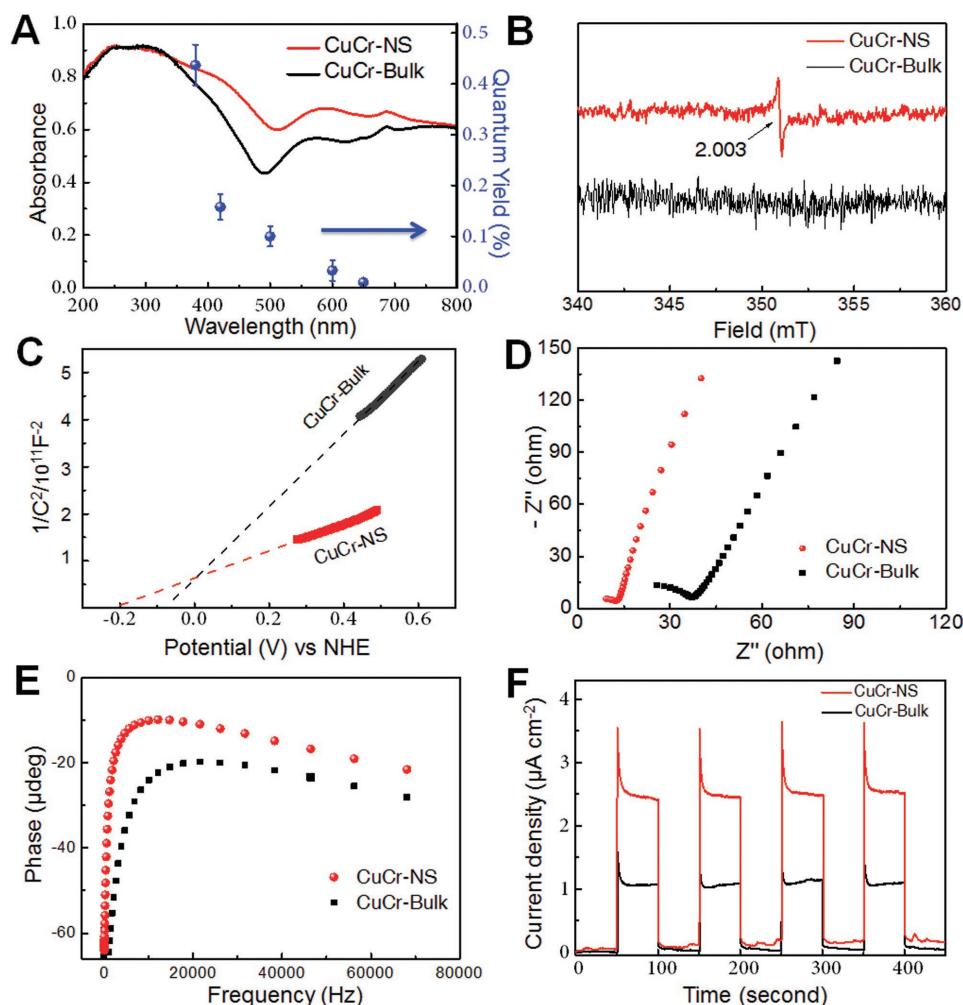
**ADVANCED
SCIENCE NEWS**

www.advancedsciencenews.com

**ADVANCED
MATERIALS**

www.advmat.de

Figure 4. A) UV–vis diffuse reflectance spectra and quantum yield for N_2 fixation over CuCr-NS under monochromatic excitation at different wavelengths (blue dots). B–F) ESR spectra (B), Mott–Schottky plot (C), EIS Nyquist plots (D), Bode phase (E), and the periodic on/off photocurrent response (F) for CuCr-NS and CuCr-Bulk.

defect structure, modified electronic structure, and resulting photoinduced charge-transfer properties. We observed that irradiation of CuCr-NS using monochromatic light of wavelengths 380, 420, 500, 600, and 650 nm can induce N_2 photoreduction, with the quantum yield determined to be ≈0.44% at 380 nm and ≈0.10% at 500 nm (**Figure 4**A). Monochromatic light of wavelength 500 nm afforded an NH_3 evolution rate of ≈7.1 µmol L^{-1} for CuCr-NS. Table S2 (Supporting Information) compares photocatalytic data for the reduction N_2 to NH_3 from the current study with prior literature data for the same reaction using different photocatalyst systems. From Table S2 (Supporting Information), it is immediately evident that the LDH photocatalysts synthesized in this work are some of the most active materials yet reported for NH_3 synthesis in pure water. Even more remarkable in this context is the activity of CuCr-NS at $\lambda > 500$ nm. On account of the outstanding activity and selectivity of CuCr-NS, an in-depth investigation of its photophysics and charge-transfer properties was undertaken. Diffuse reflectance UV–vis spectra for CuCr-NS and CuCr-Bulk are shown in Figure 4A. For

CuCr-NS, the absorption edge is red-shifted compared with that of CuCr-Bulk, allowing enhanced absorption in the visible region. Electron spin resonance (ESR) spectra revealed a difference between CuCr-NS and CuCr-Bulk (Figure 4B). CuCr-NS gives a major feature with a g-value of 2.003, which is readily assigned to an electron trapped around V_O. No such signal was observed for CuCr-Bulk. The presence of V_O in the LDH nanosheets strongly impacts their electronic structure, and also their electron transfer to adsorbates. Mott–Schottky plots were used to establish the flat band potential of the different photocatalysts. The calculated flat band potential of CuCr-NS is −0.2 V versus normal hydrogen electrode (NHE), more negative than that determined for CuCr-Bulk (−0.1 V vs NHE) (Figure 4C). Accordingly, photocatalytic N_2 reduction is more thermodynamically favorable over CuCr-NS compared with CuCr-Bulk. The effect of the band structure of CuCr-NS on the photoinduced charge-transport/transfer efficiency was explored using electrochemical impedance spectroscopy (EIS) Nyquist plots, node phase, and also the photocurrent response.[33] Figure 4D shows that CuCr-NS gives a
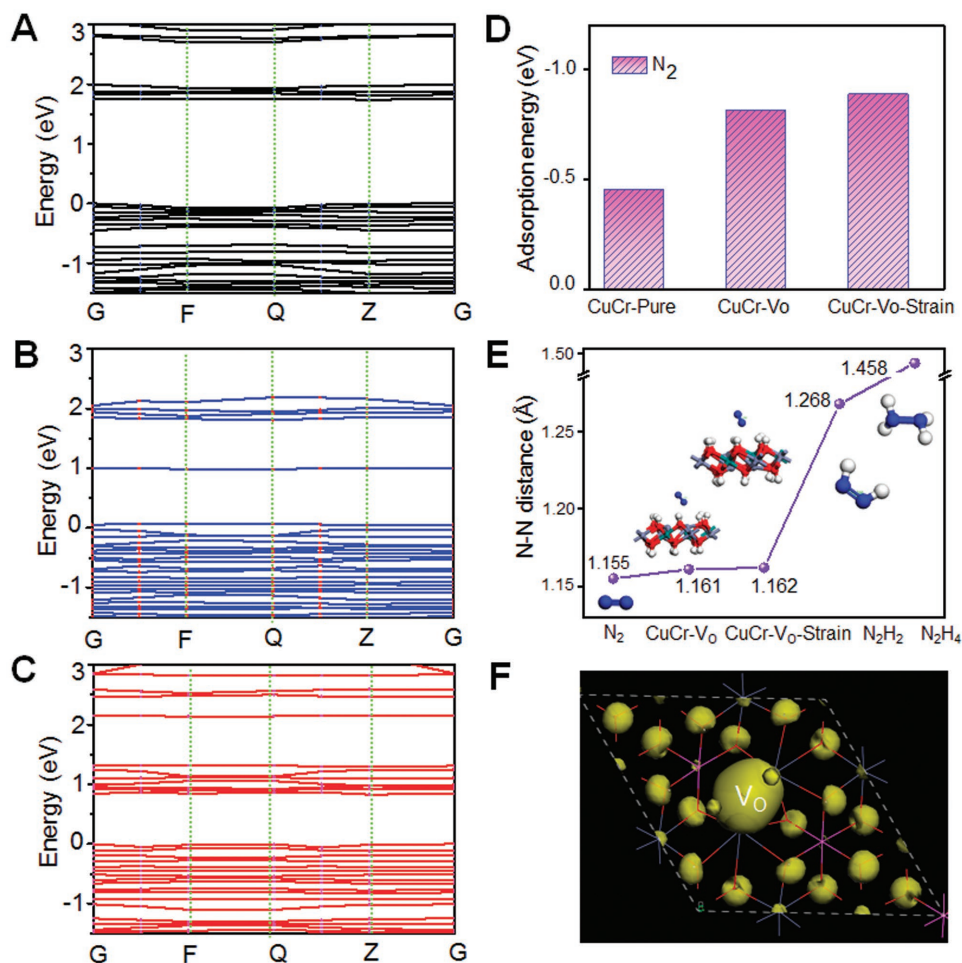
Figure 5. Band structure for CuCr-LDH with and without V_O defects: A) CuCr-Pure, B) CuCr-V_O, and C) CuCr-V_O-Strain. D) Adsorption energies of N_2 on CuCr-Pure, CuCr-V_O and CuCr-V_O-Strain. E) N−N distance of free N_2, N_2 on CuCr-V_O, N_2 on CuCr-V_O-Strain, N_2H_2, and N_2H_4. F) Charge density distribution for the VB maximum of CuCr-V_O-Strain.

significantly decreased charge-transfer resistance compared with CuCr-Bulk, which is mainly due to the high concentration of V_O in the nanosheet sample.[11b] The Bode phase of CuCr-NS also gives a longer injected electronic lifetime of 34.9 µs compared to 12.3 µs for CuCr-Bulk, calculated using the equation $(\tau = 1/(2\pi f))$,[34] where τ refers to the lifetime of the electrons and f corresponds to the minimum inverse frequency (Figure 4E). The EIS results thus confirmed the improved charge-transfer efficiency in CuCr-NS compared with CuCr-Bulk. Similar findings have previously been reported in other ultrathin systems containing surface defects and also ZnAl-LDH nanosheet systems (Figure S10, Supporting Information).[35] The enhanced light absorption and the improved charge separation efficiency lead to an increased photocurrent density in CuCr-NS (Figure 4F). These results conclusively demonstrate that V_O-rich CuCr-NS possesses a more negative conduction band (CB) and more efficient charge-transfer processes compared to CuCr-Bulk, both of which contribute to the exceptional N_2 photoreduction ability of CuCr-NS.

DFT calculations were performed to further understand the structure–activity relationship in the CuCr-LDH system. Particular emphasis was placed on the role of V_O doping and

the compressive strain within the nanosheets in enhancing photocatalytic performance. Since V_O introduces strain in CuCr-NS, we modeled the V_O-doped CuCr-LDH with a 1% compression strain (denoted as CuCr-V_O-Strain), and compared the corresponding electronic structure with that of defect-free CuCr-LDH (denoted as CuCr-Pure) and V_O-doped CuCr-LDH without strain (denoted as CuCr-V_O) (Scheme S1, Supporting Information). As shown in **Figure 5**A, the valence band (VB) maximum and CB minimum (CBM) of CuCr-Pure give a direct energy gap of about 1.6 eV, qualitatively consistent with UV–vis spectral analyses for CuCr-Bulk. After adding V_O in the LDH system, a new defect level appears in the middle of the bandgap, assigned to the existence of V_O (Figure 5B). Figure S11 (Supporting Information) shows the total and partial electronic density of states of Cr, Cu, and O in different CuCr-LDH systems. The defect level consists mainly of contributions from the unoccupied Cr 3d orbitals in LDH. After adding compressive strain in CuCr-V_O, strong defect levels form in the middle of the bandgap, which is again due to unoccupied Cr 3d orbitals (Figure 5C and Figure S11A, Supporting Information). These additional energy states likely serve as electron-trapping sites that enhance electron transfer from LDH to N_2.[16,36] Due to

differences in their surface composition and structure, the electronic structures of the CuCr-LDH with/without defects differed enormously, which in turn altered their adsorption behavior toward reactants.[37] Figure 5D revealed an increased adsorption energy for N_2 on CuCr-V_O (−0.810 eV) and CuCr-V_O-Strain (−0.886 eV) compared with defect-free CuCr-Pure (−0.453 eV). The activation of the dinitrogen triple bond is the key step in photocatalytic reduction of N_2 to NH_3 synthesis. The presence of V_O in CuCr-LDH nanosheets weakens the N_2 triple bond on chemisorption, increasing the N−N distance to 1.161 Å (compared with 1.155 Å for free molecular N_2). Introducing V_O and the strain effect further weakens the N_2 bond, giving an N−N distance of 1.162 Å (Figure 5E). Comparison of the latter with the N−N distances in N_2H_2 (1.268 Å) and N_2H_4 (1.458 Å) suggests that N_2 is adsorbed molecularly on CuCr-V_O and CuCr-V_O-Strain via coordinately unsaturated V_O sites (Figure 5F). Similarly for the ZnAl-NS system (Figure S12, Supporting Information), the N_2 adsorption energy and the N−N distance on V_O-doped ZnAl-LDH also increased compared with bulk ZnAl-LDH. The calculations suggest that V_O and the strained bonding in CuCr-NS, synergistically alter the LDH bandgap and charge-transfer efficiency following photoexcitation, thereby promoting the adsorption and photoreduction of N_2 to NH_3 in the presence of water. It should be noted that the CBM of CuCr-LDH (−0.2 V vs NHE) is at more positive potentials that required for N_2 activation (N_2/N_2H −3.2 eV vs NHE, Figure S13, Supporting Information). However, electrons photoexcited into the CB of CuCr-LDH can inject into an antibonding orbital of strongly chemisorbed N_2, thereby weakening the dinitrogen triple bond and thereby allowing NH_3 synthesis.[19b]

In summary, a series of ultrathin LDH nanosheet photocatalysts of the type $M^{II}M^{III}$-LDH (where M^{II} = Mg, Zn, Ni, Cu; and M^{III} = Al, Cr) were successfully synthesized by simple co-precipitation routes. These LDH nanosheets contained an abundance of V_O that enhanced the adsorption and activation of N_2 and H_2O, endowing the LDH nanosheets with excellent photocatalytic activity for transforming N_2 to NH_3 under UV–vis excitation and in selected cases visible excitation also (especially, CuCr-NS under wavelength > 500 nm). The introduction of Cu(II) ions in the LDH nanosheets imparted additional structural distortions and compressive strain, leading to increased interaction between the LDH and N_2, thereby promoting NH_3 evolution. This work demonstrates a promising new pathway for the reduction of N_2 to NH_3 by using LDH nanosheet photocatalysts, affording good yields of NH_3 under very mild reaction conditions. Ternary-based LDH nanosheets (like CuFeCr-LDH or ZnInAl-LDH) with their more flexible composition and electronic structures might offer superior activities for N_2 photoreduction to NH_3.

Supporting Information

Supporting Information is available from the Wiley Online Library or from the author.

Conflict of Interest

The authors declare no conflict of interest.

[1] G. Liu, H. G. Yang, J. Pan, Y. Q. Yang, G. Q. Lu, H.-M. Cheng, *Chem. Rev.* **2014**, *114*, 9559.

[2] J. X. Jian, Q. Liu, Z. J. Li, F. Wang, X. B. Li, C. B. Li, B. Liu, Q. Y. Meng, B. Chen, K. Feng, C. H. Tung, L. Z. Wu, *Nat. Commun.* **2013**, *4*, 2695.

[3] a) A. Banerjee, B. D. Yuhas, E. A. Margulies, Y. B. Zhang, Y. Shim, M. R. Wasielewski, M. G. Kanatzidis, *J. Am. Chem. Soc.* **2015**, *137*, 2030; b) J. Liu, M. S. Kelley, W. Q. Wu, A. Banerjee, A. P. Douvalis, J. S. Wu, Y. B. Zhang, G. C. Schatz, M. G. Kanatzidis, *Proc. Natl. Acad. Sci. USA* **2016**, *113*, 5530.

[4] a) K. A. Brown, D. F. Harris, M. B. Wilker, A. Rasmussen, N. Khadka, H. Hamby, S. Keable, G. Dukovic, J. W. Peters, L. C. Seefeldt, P. W. King, *Science* **2016**, *352*, 448; b) H. P. Jia, E. A. Quadrelli, *Chem. Soc. Rev.* **2014**, *43*, 547.

[5] N. Zhang, X. Li, H. Ye, S. Chen, H. Ju, D. Liu, Y. Lin, W. Ye, C. Wang, Q. Xu, J. Zhu, L. Song, J. Jiang, Y. Xiong, *J. Am. Chem. Soc.* **2016**, *138*, 8928.

[6] G. N. Schrauzer, T. D. Guth, *J. Am. Chem. Soc.* **1977**, *99*, 7189.

[7] a) H. Li, J. Shang, Z. H. Ai, L. Z. Zhang, *J. Am. Chem. Soc.* **2015**, *137*, 6393; b) H. Li, J. Shang, J. G. Shi, K. Zhao, L. Z. Zhang, *Nanoscale* **2016**, *8*, 1986; c) S. Wang, X. Hai, X. Ding, K. Chang, Y. Xiang, X. Meng, Z. Yang, H. Chen, J. Ye, *Adv. Mater.* **2017**, *29*, 1701774.

[8] X. Li, W. Wang, D. Jiang, S. Sun, L. Zhang, X. Sun, *Chem. – Eur. J.* **2016**, *22*, 13819.

[9] M. Ali, F. Zhou, K. Chen, C. Kotzur, C. Xiao, L. Bourgeois, X. Zhang, D. R. MacFarlane, *Nat. Commun.* **2016**, *7*, 11335.

[10] X.-F. Li, Q.-K. Li, J. Cheng, L. Liu, Q. Yan, Y. Wu, X.-H. Zhang, Z.-Y. Wang, Q. Qiu, Y. Luo, *J. Am. Chem. Soc.* **2016**, *138*, 8706.

[11] a) H. Duan, N. Yan, R. Yu, C. R. Chang, G. Zhou, H. S. Hu, H. Rong, Z. Niu, J. Mao, H. Asakura, T. Tanaka, P. J. Dyson, J. Li, Y. Li, *Nat. Commun.* **2014**, *5*, 3093; b) Y. Sun, S. Gao, F. Lei, C. Xiao, Y. Xie, *Acc. Chem. Res.* **2015**, *48*, 3; c) Y. F. Sun, Q. H. Liu, S. Gao, H. Cheng, F. C. Lei, Z. H. Sun, Y. Jiang, H. B. Su, S. Q. Wei, Y. Xie, *Nat. Commun.* **2013**, *4*, 2899; d) Y. F. Sun, Z. H. Sun, S. Gao, H. Cheng, Q. H. Liu, J. Y. Piao, T. Yao, C. Z. Wu, S. L. Hu, S. Q. Wei, Y. Xie, *Nat. Commun.* **2012**, *3*, 1057.

[12] a) M. L. Guan, C. Xiao, J. Zhang, S. J. Fan, R. An, Q. M. Cheng, J. F. Xie, M. Zhou, B. J. Ye, Y. Xie, *J. Am. Chem. Soc.* **2013**, *135*,

ADVANCED
SCIENCE NEWS
www.advancedsciencenews.com

ADVANCED
MATERIALS
www.advmat.de

10411; b) H. Li, J. Li, Z. Ai, F. Jia, L. Zhang, *Angew. Chem., Int. Ed.*, https://doi.org/10.1002/ange.201705628.

[13] a) H. Han, H. Frei, *J. Phys. Chem. C* **2008**, *112*, 8391; b) D. Bruhwiler, H. Frei, *J. Phys. Chem. B* **2003**, *107*, 8547; c) H. Han, H. Frei, *J. Phys. Chem. C* **2008**, *112*, 16156; d) R. Nakamura, A. Okamoto, H. Osawa, H. Irie, K. Hashimoto, *J. Am. Chem. Soc.* **2007**, *129*, 9596.

[14] a) L. Mohapatra, K. Parida, M. Satpathy, *J. Phys. Chem. C* **2012**, *116*, 13063; b) L. Mohapatra, K. Parida, *J. Mater. Chem. A* **2016**, *4*, 10744.

[15] a) Q. Wang, D. O'Hare, *Chem. Rev.* **2012**, *112*, 4124; b) Y. F. Zhao, X. Jia, G. I. N. Waterhouse, L. Z. Wu, C. H. Tung, D. O'Hare, T. R. Zhang, *Adv. Energy Mater.* **2016**, *6*, 1501974; c) C. Gomes Silva, Y. Bouizi, V. Fornes, H. Garcia, *J. Am. Chem. Soc.* **2009**, *131*, 13833; d) K. Teramura, S. Iguchi, Y. Mizuno, T. Shishido, T. Tanaka, *Angew. Chem., Int. Ed.* **2012**, *51*, 8008; e) J. L. Gunjakar, T. W. Kim, H. N. Kim, I. Y. Kim, S. J. Hwang, *J. Am. Chem. Soc.* **2011**, *133*, 14998; f) R. Ma, T. Sasaki, *Acc. Chem. Res.* **2015**, *48*, 136.

[16] Y. Zhao, G. Chen, T. Bian, C. Zhou, G. I. Waterhouse, L. Z. Wu, C. H. Tung, L. J. Smith, D. O'Hare, T. Zhang, *Adv. Mater.* **2015**, *27*, 7824.

[17] a) G. Ertl, *Angew. Chem., Int. Ed.* **2008**, *47*, 3524; b) D. Zhu, L. H. Zhang, R. E. Ruther, R. J. Hamers, *Nat. Mater.* **2013**, *12*, 836; c) H. Z. Liu, *Chin. J. Catal.* **2014**, *35*, 1619; d) P. Wang, F. Chang, W. Gao, J. Guo, G. Wu, T. He, P. Chen, *Nat. Chem.* **2017**, *9*, 64; e) C. J. M. van der Ham, M. T. M. Koper, D. G. H. Hetterscheid, *Chem. Soc. Rev.* **2014**, *43*, 5183; f) I. Coric, B. Q. Mercado, E. Bill, D. J. Vinyard, P. L. Holland, *Nature* **2015**, *526*, 96.

[18] a) J. Li, H. Li, G. Zhan, L. Zhang, *Acc. Chem. Res.* **2017**, *50*, 112; b) A. J. Medford, M. C. Hatzell, *ACS Catal.* **2017**, *7*, 2624; c) Y. Zhao, B. Zhao, J. Liu, G. Chen, R. Gao, S. Yao, M. Li, Q. Zhang, L. Gu, J. Xie, X. Wen, L. Z. Wu, C. H. Tung, D. Ma, T. Zhang, *Angew. Chem., Int. Ed.* **2016**, *55*, 4215.

[19] a) J. Li, G. Zhan, Y. Yu, L. Zhang, *Nat. Commun.* **2016**, *7*, 11480; b) H. Hirakawa, M. Hashimoto, Y. Shiraishi, T. Hirai, *J. Am. Chem. Soc.* **2017**, *139*, 10929; c) S.-J. Li, D. Bao, M.-M. Shi, B.-R. Wulan, J.-M. Yan, Q. Jiang, *Adv. Mater.* **2017**, *29*, 1700001.

[20] J. D. Egbert, M. O'Hagan, E. S. Wiedner, R. M. Bullock, N. A. Piro, W. S. Kassel, M. T. Mock, *Chem. Commun.* **2016**, *52*, 9343.

[21] a) Y. Zhao, F. Li, R. Zhang, D. G. Evans, X. Duan, *Chem. Mater.* **2002**, *14*, 4286; b) J. He, M. Wei, B. Li, Y. Kang, D. G. Evans,

[22] a) H. Li, J. Wu, Z. Yin, H. Zhang, *Acc. Chem. Res.* **2014**, *47*, 1067; b) V. Nicolosi, M. Chhowalla, M. G. Kanatzidis, M. S. Strano, J. N. Coleman, *Science* **2013**, *340*, 1420; c) C. Tan, H. Zhang, *Nat. Commun.* **2015**, *6*, 7873.

[23] Y. Zhao, B. Li, Q. Wang, W. Gao, C. J. Wang, M. Wei, D. G. Evans, X. Duan, D. O'Hare, *Chem. Sci.* **2014**, *5*, 951.

[24] L. Yang, X. Cui, J. Zhang, K. Wang, M. Shen, S. Zeng, S. A. Dayeh, L. Feng, B. Xiang, *Sci. Rep.* **2014**, *4*, 5649.

[25] H. Roussel, V. Briois, E. Elkaim, A. de Roy, J. P. Besse, *J. Phys. Chem. B* **2000**, *104*, 5915.

[26] a) B. M. Weckhuysen, I. E. Wachs, R. A. Schoonheydt, *Chem. Rev.* **1996**, *96*, 3327; b) Y. Zhao, S. Zhang, B. Li, H. Yan, S. He, L. Tian, W. Shi, J. Ma, M. Wei, D. G. Evans, X. Duan, *Chem.– Eur. J.* **2011**, *17*, 13175.

[27] W. Y. Lin, H. Frei, *J. Am. Chem. Soc.* **2005**, *127*, 1610.

[28] N. Baliarsingh, L. Mohapatra, K. Parida, *J. Mater. Chem. A* **2013**, *1*, 4236.

[29] S.-M. Xu, T. Pan, Y.-B. Dou, H. Yan, S.-T. Zhang, F.-Y. Ning, W.-Y. Shi, M. Wei, *J. Phys. Chem. C* **2015**, *119*, 18823.

[30] a) A. Zecchina, L. Marchese, S. Bordiga, C. Pazè, E. Gianotti, *J. Phys. Chem. B* **1997**, *101*, 10128; b) J. N. Kondo, S. Shibata, Y. Ebina, K. Domen, A. Tanaka, *J. Phys. Chem.* **1995**, *99*, 16043.

[31] F. Giraud, C. Geantet, N. Guilhaume, S. Gros, L. Porcheron, M. Kanniche, D. Bianchi, *J. Phys. Chem. C* **2014**, *118*, 15664.

[32] T. Cuk, W. W. Weare, H. Frei, *J. Phys. Chem. C* **2010**, *114*, 9167.

[33] J. S. Zhang, X. F. Chen, K. Takanabe, K. Maeda, K. Domen, J. D. Epping, X. Z. Fu, M. Antonietti, X. C. Wang, *Angew. Chem., Int. Ed.* **2010**, *49*, 441.

[34] S. Sun, W. Wang, L. Zhang, *J. Phys. Chem. C* **2013**, *117*, 9113.

[35] Y. F. Sun, Z. H. Sun, S. Gao, H. Cheng, Q. H. Liu, F. C. Lei, S. Q. Wei, Y. Xie, *Adv. Energy Mater.* **2014**, *4*, 1300611.

[36] H. Li, C. Tsai, A. L. Koh, L. Cai, A. W. Contryman, A. H. Fragapane, J. Zhao, H. S. Han, H. C. Manoharan, F. Abild-Pedersen, J. K. Norskov, X. Zheng, *Nat. Mater.* **2016**, *15*, 48.

[37] A. Castellanos-Gomez, R. Roldan, E. Cappelluti, M. Buscema, F. Guinea, H. S. J. van der Zant, G. A. Steele, *Nano Lett.* **2013**, *13*, 5361.

1703828 (10 of 10)